Seismic Assessment of Trapezoidal-Shaped Hills Induced by Strong Ground Motion Records

Masoud Amelsakhi[1*], Abdollah Sohrabi-Bidar[2], and Arash Shareghi[3]

1. Assistant Professor, Department of Civil Engineering, Faculty of Engineering and Technology, Qom University of Technology, * Corresponding Author; email: amelsakhi@qut.ac.ir
2. Associate Professor, School of Geology, College of Science, University of Tehran
3. Department of Civil Engineering, Faculty of Engineering, Urmia University

Received: 10/10/2017
Accepted: 28/04/2018

ABSTRACT

This study aims to rigorously examine the influences of the vertically propagating recorded strong ground motions on the trapezoidal-shaped hills in different sizes and shape ratios. In order to generalize the results of the study, one-dimensional as well as two-dimensional analyses are conducted. Then, intended results are represented in dimensionless form as a result of which amplification ratio patterns are extracted and compared with each other in terms of displacement, velocity, and acceleration. Similarly, corresponding response spectra ratios are derived on significant points on hill-crest, hill-side, and beside of that, and juxtaposed in diagrams. Results of the assessment are put together with that of recent studies and predictions of the reliable codes. An adequate agreement between maximum values of amplification ratios obtained in time-domain analyses and spectral analyses makes us hopeful to think of connecting time-domain parameters with spectra-related ones to propose an accurate equation, which considers more effective variations regarding the topographic seismic effects and gives most reliable prediction. However, here, an equation has already been suggested to draw amplification ratio patterns on different points of the hill for a limited hill-shape, dimension, media characterization and constitutive model. Comparing the estimations of the amplification ratio patterns using different methods proves that, considering potent parameters related to the time-domain and frequency-domain, the proposed equation is more efficient than the other codes.

Keywords:
Topographic effect; Time-domain amplification ratio; Spectral amplification ratio, Geotechnical earthquake engineering

1. Introduction

Recent evaluations of recorded ground motions and construction damages during the earthquakes have demonstrated significant influences of surface irregularities on patterns of surface wave propagation. Researchers' observations during 1983 Coalinga earthquake [1], 1985 Chile earthquake [2], 1987 Superstition Hills earthquake [1], and 1999 Greece earthquake [3-4] and recorded accelerations in Pacoima Dam during 1971 San Fernando earthquake [5-6] and Tarzana Hill (1.78 g) during 1994 Northridge earthquake [7] are some examples of the earthquake events where topography had an effective role in damage distributions.

Boore [8] used finite difference method to evaluate the triangle-shaped hill induced by SH waves. Bouchon [9] studied the semi-sine shaped hill in different shape ratios by scattering SH waves. Bard [10] studied scattering and propagating of *P* and SV waves on surface irregularities. Sanchez-Sesma [11] evaluated the diffraction and dispersion of SH waves on triangle shaped hill. Bouchon [12] and Gaffet and Bouchon [13] used discrete

wave-number boundary element method to study *P*, *SV* and *SH* wave propagations on surface topographies. Sanchez-Sesma and Campillo [14-15] studied the seismic behavior of semi-elliptical and triangle-shaped hills under propagation of *P* and *SV* waves using boundary element method in frequency domain. Ashford et al. [16] performed a frequency-domain parametric study using generalized consistent transmitting boundaries to evaluate the significance of topographic effects on seismic response of steep slopes. They successfully separated the topography induced amplification from natural frequency origin amplification that can be used to develop a simplified method to estimate topographic effects. Zhang et al. [17] used hybrid discrete wave-number boundary element and finite element method to scatter *SV* waves to the trapezoidal-shaped hill. Bouckovalas and Papadimitriou [18] conducted numerical analyses for the seismic response of step-like ground slopes in uniform viscoelastic soil under vertically propagation of *SV* seismic waves. Kamalian et al. [19-20] conducted a comprehensive study using boundary element method and hybrid boundary element and finite element method on two-dimensional semi-sine, semi-elliptical, and trapezoidal-shaped hills under vertically propagating *P* and *SV* waves. In addition, Kamalian et al. [21] studied different parameters such as incident wave length, shape ratio, Poisson ratio and hill shape on ground amplifications under vertically propagating of *SV* Ricker wave. Sohrabi-Bidar [22] and Sohrabi-Bidar et al. [23-25] used three-dimensional boundary element method to study different shapes of surface irregularities in time domain. Furthermore, Sohrabi-Bidar and Kamalian [26] assessed the seismic behavior of the 2D and 3D Gaussian-shaped hill. They showed that wavelength, shape ratio, dimension ratios, and wave type are the key independent parameters governing the amplifying behavior of the hills.

The concept of a response spectra was first introduced by Housner [27] and Biot [28]. Spectra have been widely used for the purposes of differentiating the significant characteristics of accelerogram records and provided a simple method of evaluating the seismic response of all types of structure. Housner [29], Hayashi et al. [30], Mohraz et al. [31], Blume et al. [32], Newmark et al. [33], Seed et al. [34] and many others extensively studied the response spectra of the different types of sites induced by different earthquake records. Nonetheless, all these investigations were based on the results of one-dimensional analysis. The extensive experimental studies conducted by Borcherdt [35-36] showed that the short period site coefficient could be approximated as the spectral amplification averaged over the period interval 0.1 to 0.5 second, whereas the moderately long period site coefficient could be approximated as the spectral amplification averaged over the period interval 0.4 to 2.0 second.

Assimaki et al. [37] introduced the concept of 2D over 1D response spectral ratio to describe the effects of topography as a function of local soil conditions. They suggested a frequency and location-dependent topographic aggravation factor to be introduced for the modification of design spectra in a seismic code. Kamalian et al. [38] estimated the seismic site coefficients for the crest of the semi-elliptical shaped hills with various shape ratios that were period dependent and therefore more representative of the amplification pattern of 2D hills, whereas the constant topography factors proposed by AFPS [39] and Eurocode [40] do not take this important controlling factor into account.

In this study, different sizes of the trapezoidal-shaped hills with different shape ratios analyzed under vertically propagating of the far-fault earthquake records. Then, in order to gain a dimensionless form of results, their amplifications on the ground in two-dimensional models were divided to their corresponding amplifications in free field in time domain. For further investigation, response spectra on significant points on the hills and besides were compared with each other. Then, the results of spectral assessing were used to correct the amplification ratios presented in time domain.

2. Methodology of Parametric Study

Numerical modeling conducted using finite difference method implemented in FLAC2D to evaluate the effects of ground motion records on seismic behavior of the trapezoidal shaped hills. It should be noted that the explicit method in this software is used to solve the models that is appropriate for dynamic analyses. In order to verify the feasibility of the numerical method for seismic

analyses of topographic structures, response of a particular case of a canyon in the linear visco-elastic soil has been calculated. As shown in Figure (1), the canyon has the radius of R = 25 meters and the medium soil has the shear wave velocity of Vs = 500 m/s, the Poisson's ratio of $\upsilon = 1/3$, and the mass density of $\rho = 2000$ kg/m^3. The canyon has been excited by the vertically propagating SV wave of Ricker type, the displacement equation of which is as follows:

$$f(t) = A_{\max}\left[1-2\left(\pi.f_p\left(t-t_0\right)\right)^2\right].e^{-\left(\pi.f_p\left(t-t_0\right)\right)^2} \quad (1)$$

A typical comparison between numerical and analytical predictions [41] for the horizontal (Uh) and the vertical (Uv) components of the normalized peak ground surface displacement versus dimensionless distance is shown in Figure (2), where L is width of valley and X is distance away from valley center.

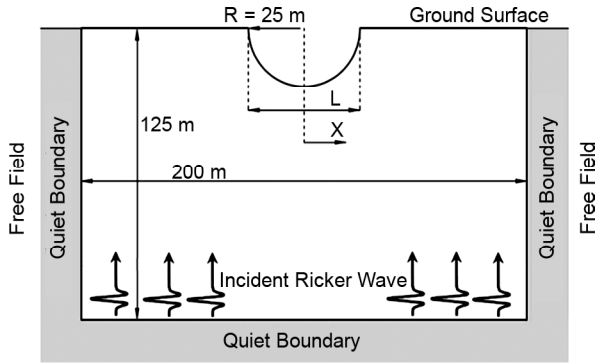

Figure 1. Typical model of the canyon of 25 m radius, the total dimension and applied boundary conditions.

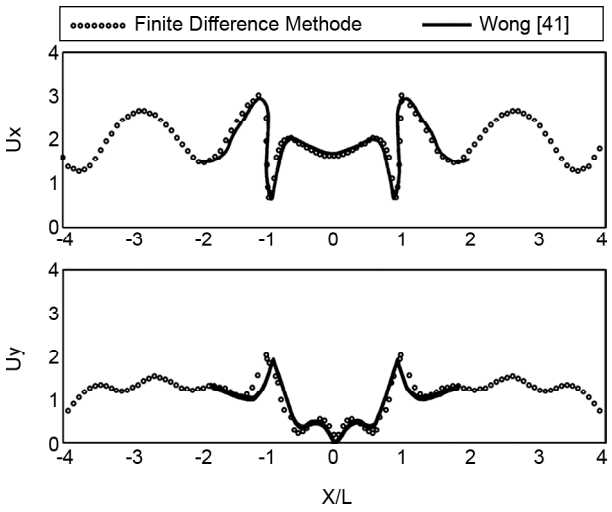

Figure 2. Numerical results for the canyon topography in comparison with analytical solution in terms of the normalized peak ground surface displacement [41].

In order to parametrically evaluate the trapezoidal-shaped hills, shape ratios (SR) of 0.1, 0.3, 0.5, and 0.7 with the hill-width (B) of 200,400 and 600 meters and slope of 45 degrees have been considered. In this study, the results have presented for specific case of uniform site material with VS= 760 m/s, Poisson's ratio $\upsilon = 0.4$ (Elasticity modulus E=4 GPa) and mass density ρ=2400 kg/m^3. A schematic illustration of the 2D analyzed model and the boundary conditions are presented in Figure (3). To reduce the effects of artificial wave reflections from the boundaries at the area of interest, the height of the model sizes is set at least to 5H [18]. In addition, the width of the models is set to $8\times(B/2)$, the distance from which the topographic effects more or less dissipate, i.e. the peak ground surface response of 2D analyses and 1D analyses (free field) become almost compatible. To apply dynamic damping, Rayleigh method is used by defining two parameters, central frequency and critical damping ratio. Critical damping ratio is set to be 0.05 that is practical for rocky media. Besides, central frequencies have considered to be the same as the natural period of the models (lowest free vibration frequency of whole 2D model) which had been obtained from the modal analyses of the 2D models. For gaining the natural period of the models, 2D simulations are performed and analyzed in ANSYS software.

To exclude other causes of amplification except the topography-induced amplification, the results have been represented in dimensionless amplification ratio forms. The amplification ratios are obtained by dividing the values of the surface peak ground motion of 2D analyses to that of 1D profile analyses with the same properties at each specific point. The 1D profiles at the different

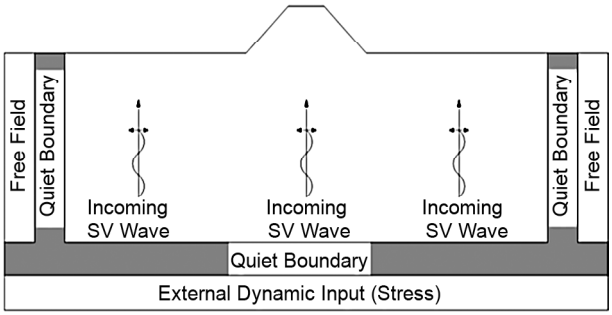

Figure 3. Schematic illustration of finite difference model for a two-dimensional trapezoidal-shaped topography.

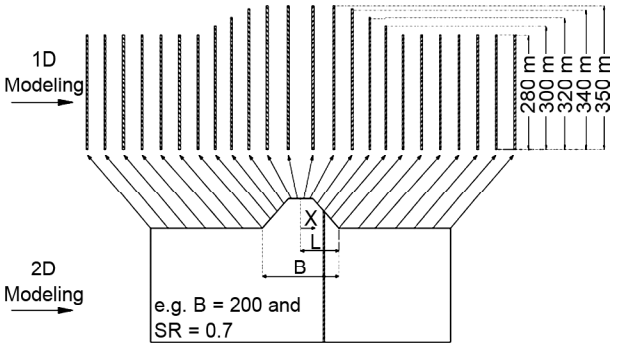

Figure 4. Schematic illustration of one-dimensional profile models at different points on the trapezoidal-shaped hill with 0.7 shape ratio and 200 m hill-width.

points on the surface for the hill of 200 m width and 0.7 shape ratio are shown in Figure (4). The 1D models have analyzed using FLAC software as well.

Then, the models have induced by vertically propagating of twelve far-fault strong ground motion records listed in Table (1). It should be mentioned that far-fault records are selected using IBC [42] criteria according to which moderate magnitude range of 6-7.5, epicenteric distance more than 20 km, PGA range of 0.8-1.86 m/s^2, and site classification of shear wave velocity more than (Vs) 750 m/s are taken into account.

To apply the mesh sensitivity for the models, Kuhlemeyer and Lysmer [43] criteria was satisfied. Subsequently, all dimensions of the mesh should be less than $\lambda/10$, where λ is incident earthquake record wavelengths as a result of which specific range of the frequencies are filtered. To do so, Chebyshev low pass filtering applied using SeismoSignal software.

3. Results and Discussion

3.1. Time Domain Results

The average amplification ratios of ground motion parameters are shown in Figures (5) and (6). To do so, the twelve earthquake records used as excitation and the results are shown for a 200-meter-wide hill and for different shape ratios (SR), defined as the ratio of height of the hill on the half-width of the hill. The amplification ratios are obtained by dividing the peak ground acceleration (also velocity and displacement) of the horizontal component of the motion resulted from 2D analysis to the corresponding peak ground acceleration (also velocity and displacement) in free field (1D analysis). It can be seen that the amplification ratio pattern increases as the shape ratio of the hill increases from 0.1 to 0.7. Raising the amplification ratio pattern governs in all ground motion parameters, acceleration, velocity, and displacement; however, the amount of values are different. The aggravating effect of topography on the hill decreases as the ground motion parameter changes from acceleration to velocity and from velocity to displacement. The amplification ratios at different surficial points on the crest of the hill with the shape ratio of 0.7 and the hill-width of 200 m reaches up to 1.6, 1.4, and 1.2 for acceleration, velocity, and displacement, respectively.

When the hill enlarges, it increases in B, the influence of topography on velocity and displacement seems to be more than its effect on acceleration. In other words, the acceleration amplification ratio do not change notably, while the velocity amplification

Table 1. Far-fault earthquake records and station details adapted from PEER strong motion database [44].

Earthquake Event - Date	Station / Component (deg)	Site Classification (USGS)	Magnitude (M)	Distance (km)	PGA (m/s^2)	PGV (cm/s)	PGD (cm)
Landers - 1992/06/28	Amboy / 90	A > 750 m/s	7.3	69.2	1.40	18.59	6.81
Loma Prieta - 1989/10/18	San Francisco, Sierra Pt. / 205	A > 750 m/s	6.9	68.2	0.80	9.41	1.96
Northridge - 1994/01/17	Lake Hughes #9 / 0	A > 750 m/s	6.7	26.8	1.70	5.99	1.95
Northridge - 1994/01/17	LA - Wonderland Ave. / 185	A > 750 m/s	6.7	22.7	1.70	13.71	2.03
Northridge - 1994/01/17	Mt Wilson - CIT SeisSta. / 0	A > 750 m/s	6.7	36.1	1.86	7.80	0.55
Northridge - 1994/01/17	Leona Valley #3 / 90	A > 750 m/s	6.7	37.8	0.83	6.89	1.88
Northridge - 1994/01/17	San Gabriel - Grand Ave. / 180	A > 750 m/s	6.7	41.7	1.43	7.33	1.33
N. Palm Springs - 1986/07/08	Anza - Red Mountain / 360	A > 750 m/s	6.0	45.6	1.05	3.37	0.43
N. Palm Springs - 1986/07/08	Silent Valley - Poppet F. / 0	A > 750 m/s	6.0	25.8	0.96	2.83	0.47
San Fernando - 1971/02/09	Lake Hughes #9 / 21	A > 750 m/s	6.6	23.5	0.88	5.49	0.62
Victoria, Mexico - 1980/06/09	SAHOP Casa Flores / 90	A > 750 m/s	6.0	21.2	1.46	4.73	0.23
Whittier Narrows - 1987/10/01	Mt Wilson - CIT SeisSta. / 10	A > 750 m/s	6.1 (ML)	58.3	1.10	6.19	1.41

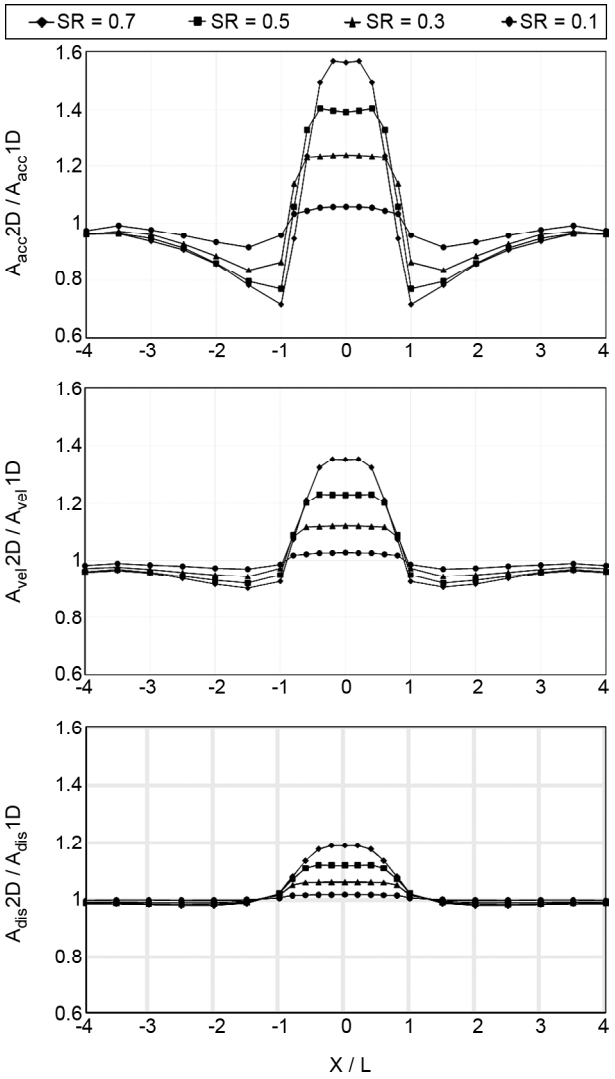

Figure 5. Shape ratio effect. The amplification ratios at different points on the ground surface in terms of horizontal acceleration, velocity, and displacement; for the hills of 200 m wide and various shape ratios; the amplification ratio patterns are averaged for the twelve strong ground motion records.

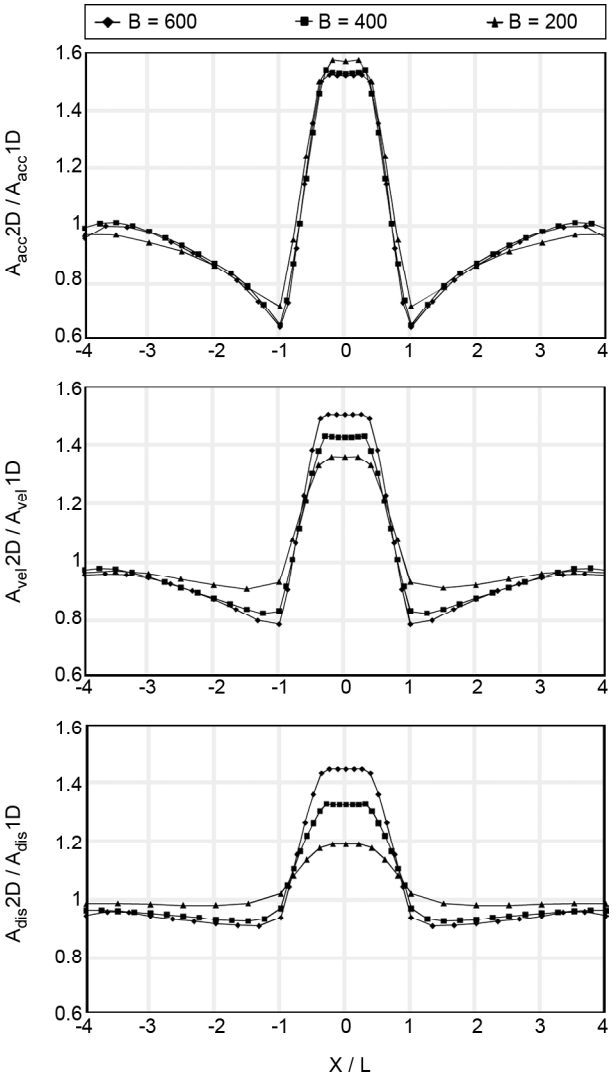

Figure 6. Hill-width effect. The amplification ratios at different points on the ground surface in terms of horizontal acceleration, velocity, and displacement; for the hills with 0.7 shape ratio and various hill-widths; the amplification ratio patterns are averaged for the twelve strong ground motion records.

ratio raises, and even, the displacement amplification ratio raises more than that of velocity. This is due to the fact that displacement records have longer wavelength than that of velocity, and also velocity records have longer wavelength than that of acceleration; thus, it is expected that the increase in hill-width is to amplify longer wavelengths.

Acceleration is less sensitive to the increase in hill-width when it comes to compare with velocity and displacement. Figure (7) shows a correlation between the acceleration amplification ratios of the crest of the trapezoidal hills, averaged over the twelve far-fault earthquake records, and shape ratios of the hill. This correlation is simplified to a linear function (Equation 2) as follows:

$$A_{acc}\left(2D/1D\right)=1+0.8\left(SR\right) \tag{2}$$

3.2. Response Spectra

To assess the topographic effects on seismic behavior of the trapezoidal-shaped hill in terms of the response spectra of the linear single-degree-of-freedom (SDOF) oscillators, points A ($X/L=0$), B ($X/L=0.3$), C ($X/L=1$), and D ($X/L=2$) are selected at specific distances from the hill center. Then, in the cases of the hills of different shape ratios (0.1, 0.3, 0.5, and 0.7) and hill widths (200, 400, and 600 m), their acceleration, velocity and displacement response spectra, resulted from 1D and 2D analyses are compared with each other.

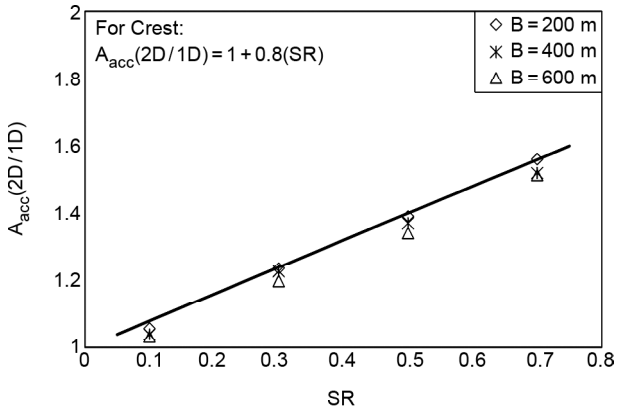

Figure 7. The relation between the maximum amplification ratios at the crest of the trapezoidal shaped hills for different hill-widths and shape ratios

To do so, response spectra for all the twelve records at considered points (*A*, *B*, *C*, and *D*) are calculated for 1D and 2D modeling. And then, the mean spectrum is determined to be a representative curve. For instance, as it is shown in Figure (8), at the first step (a), the mean spectrum out of the twelve records resulted from one-dimensional analysis is determined; and at the second step (b), the mean spectrum out of the twelve records resulted from two-dimensional analysis is calculated, and finally (c), the result of stage two divided by that of stage one makes the representative spectral amplification curve.

In order to distinguish the outstanding differences of two-dimensional analysis-type with the one-dimensional one, Figure (9) is presented in terms of spectra that illustrates the spectral amplification ratio curves for acceleration, velocity, and displacement at the points *A*, *B*, *C*, and *D* on the hills of 0.7 shape ratio and different hill widths. In general, the spectral amplification ratio curves at the points *A* and *B* have more or less values higher than one that means spectral amplification for all periods, except those of less than 0.3. On the other hand, at the points *C* and *D*, located at the toe of hills, de-amplification mostly is observed. Formerly, these amplifications and de-amplifications have been noticed in time domain assessments by others [19-20, 26, 38, 45-46]. As it is clear in Figure (9), the larger the hill becomes, the wider the topography affected period intervals extend, i.e. amplification at the points on the crest of the hill and de-amplification at the points on the hill toe influence on longer period intervals, and also, the greater, in the cases of the

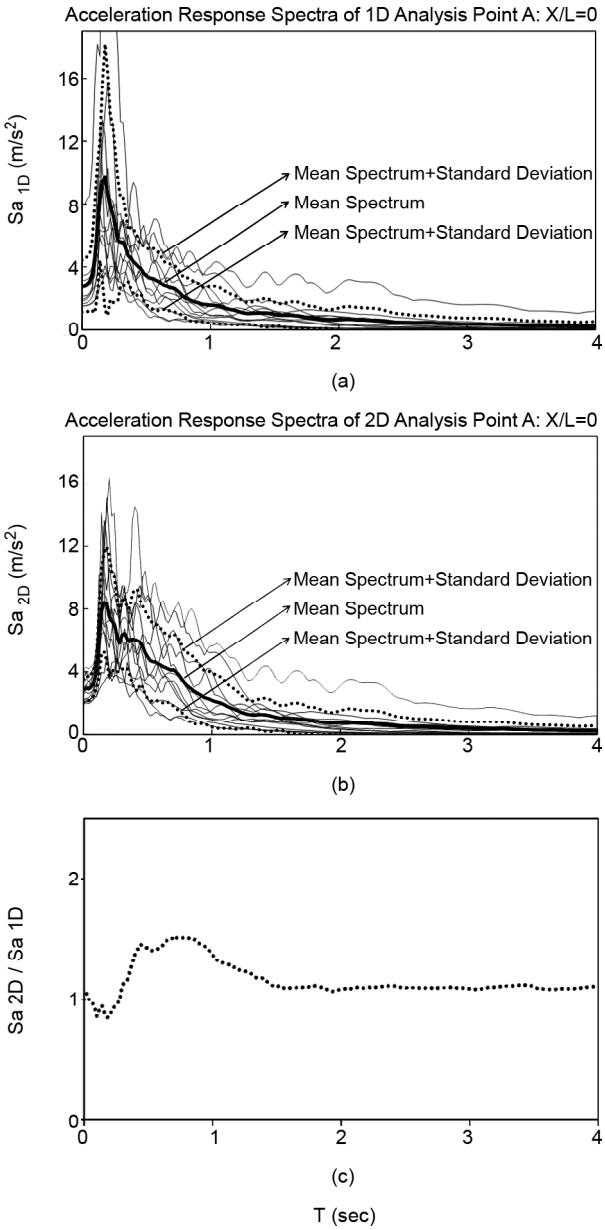

Figure 8. Acceleration response spectra resulted from 1D analyses (a) and 2D analyses (b) and the representative spectral amplification ratio curve (c) at center of the crest (point A) for a trapezoidal-shaped hill with the shape ratio of 0.7 and the hill-width of 200 m.

points *A* and *B*, the spectral amplification ratio values show.

According to the engineering considerations, an incident wave, the wavelength of which is 0.25 to 8.33 times the width of the hill, has enough susceptibility to be affected by the ground surface irregularities in a remarkable manner. Here, this broad period interval is divided into the following ten sub-intervals: 0.25 - 0.5 (*P*1), 0.5 - 1.0 (*P*2), 1.0 - 1.5 (*P*3), 1.5 - 2.0 (*P*4), 2.0 - 3.0 (*P*5), 3.0 - 4.0 (*P*6), 4.0 - 5.0 (*P*7), 5.0 - 6.0 (*P*8), 6.0 - 7.0 (*P*9), and 7.0 - 8.0 (*P*10). To generalize the discussion,

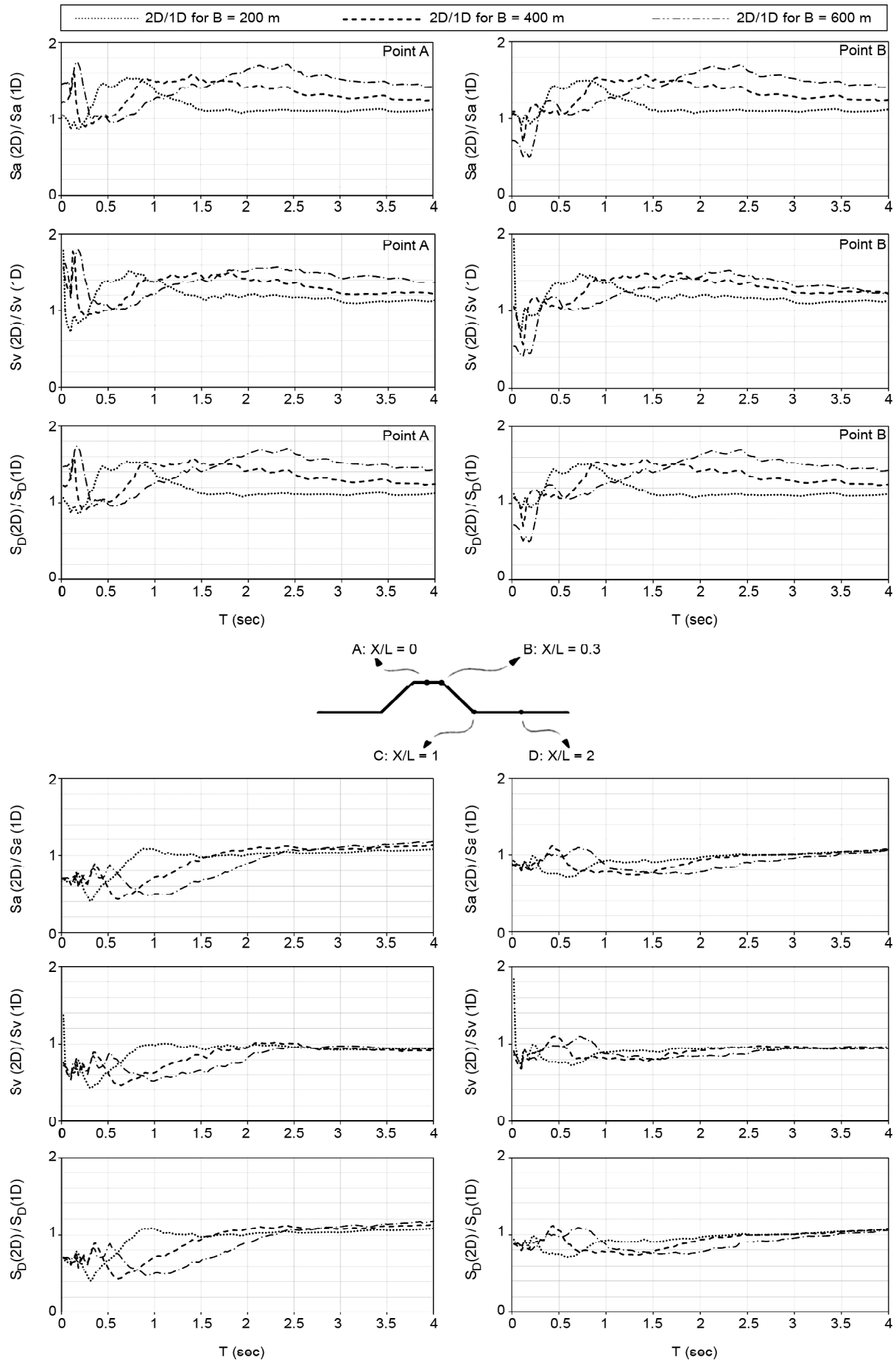

Figure 9. Acceleration, velocity and displacement response spectra ratios resulted of 2D and 1D analyses at points A, B, C and D; for 0.7 shape ratio and various hill widths; averaged for 12 strong ground motion records.

dimensionless period sub-interval is defined as a ratio in which the amount of the wavelength of the incident motion is divided to that of the hill-width. Table (2) presents period sub-intervals calculated for the three different hill-widths and ten P_i (dimensionless period sub-intervals).

Tables (3) and (4) have calculated for the diagrams related to the points *A* and *B* in Figure (9) with a corresponding classification presented in Table (2). Putting all the results of Tables (3) and (4), amplification ratios in spectral-domain; that of Figures (5) and (6), amplification ratios in time-domain; and that of Kamalian et al. [21], conducted in spectral-domain by means of propagating *SV* wave of the Ricker type, together, one can clearly see an agreement among the amplification ratio values. Elaborately speaking, the maximum amplification ratio values shown in Figures (5) and (6) are compatible with those presented in Tables (3) and (4) in dimensionless period sub-interval 2 - 4

Table 2. Period sub-intervals (second) for the three different hill-widths and dimensionless period sub-intervals.

(B)	Dimensionless Period Sub-Interval									
	P1 0.25-0.5	P2 0.5-1.0	P3 1.0-1.5	P4 1.5-2.0	P5 2.0-3.0	P6 3.0-4.0	P7 4.0-5.0	P8 5.0-6.0	P9 6.0-7.0	P10 7.0-8.0
200	0.6–0.13	0.13–0.26	0.26–0.39	0.39–0.53	0.53–0.79	0.79–1.05	1.05–1.31	1.31–1.58	1.58–1.84	1.84–2.10
400	0.13–0.26	0.26–0.53	0.53–0.79	0.79–1.06	1.06–1.58	1.58–2.10	2.10–2.63	2.63–3.16	3.16–3.68	3.68–4.21
600	0.20–0.39	0.39–0.79	0.79–1.18	1.18–1.58	1.58–2.37	2.37–3.16	3.16–3.95	3.95–4.73	4.73–5.52	5.52–6.32

Table 3. Spectral amplification ratios of the point at the hill crest (point A) for different shape ratios, hill widths, and dimensionless period sub-intervals.

SR	Hill-Width (B)	Dimensionless Periodic Sub-Interval									
		P1	P2	P3	P4	P5	P6	P7	P8	P9	P10
0.1	200	-	-	1.0	1.0	1.0	1.0	1.0	0.9	1.0	1.0
	400	-	1.0	1.0	1.0	1.0	1.0	1.0	1.0	1.1	-
	600	0.8	1.0	1.1	1.0	1.0	1.1	1.1	-	-	-
0.3	200	-	-	1.1	1.2	1.1	1.1	1.0	1.0	1.0	1.0
	400	-	1.1	1.1	1.2	1.1	1.1	1.1	1.1	1.1	-
	600	1.0	1.1	1.2	1.2	1.2	1.2	1.2	-	-	-
0.5	200	-	-	1.2	1.3	1.3	1.3	1.2	1.1	1.0	1.1
	400	-	1.1	1.2	1.4	1.3	1.3	1.2	1.2	1.2	-
	600	0.7	1.1	1.3	1.3	1.4	1.4	1.3	-	-	-
0.7	200	-	-	1.2	1.4	1.5	1.5	1.3	1.1	1.1	1.1
	400	-	1.0	1.2	1.5	1.5	1.5	1.4	1.3	1.3	-
	600	1.2	1.0	1.2	1.4	1.6	1.6	1.5	-	-	-

Table 4. Spectral amplification ratios of the point at top edge of the hill slope (point B) for different shape ratios, hill widths, and dimensionless period sub-intervals.

SR	Hill-Width (B)	Dimensionless Periodic Sub-Interval									
		P1 0.25-0.5	P2 0.5-1.0	P3 1.0-1.5	P4 1.5-2.0	P5 2.0-3.0	P6 3.0-4.0	P7 4.0-5.0	P8 5.0-6.0	P9 6.0-7.0	P10 7.0-8.0
0.1	200	-	-	0.9	1.0	0.9	1.0	1.0	0.9	1.0	1.0
	400	-	0.9	1.0	1.0	1.0	1.0	1.0	1.0	1.1	-
	600	0.9	0.9	1.0	1.0	1.0	1.1	1.1	-	-	-
0.3	200	-	-	1.1	1.2	1.1	1.1	1.0	1.0	1.0	1.0
	400	-	1.0	1.2	1.2	1.1	1.1	1.1	1.1	1.1	-
	600	0.9	1.0	1.2	1.2	1.2	1.2	1.2	-	-	-
0.5	200	-	-	1.2	1.3	1.3	1.3	1.2	1.1	1.0	1.1
	400	-	1.1	1.2	1.4	1.3	1.3	1.2	1.2	1.2	-
	600	0.7	1.1	1.3	1.3	1.4	1.4	1.3	-	-	-
0.7	200	-	-	1.2	1.4	1.5	1.4	1.3	1.1	1.1	1.1
	400	-	1.1	1.2	1.5	1.5	1.5	1.4	1.3	1.3	-
	600	1.0	1.1	1.2	1.4	1.6	1.6	1.5	-	-	-

(*P*5 and *P*6), and also with those presented in Kamalian et al. [21] studies over the dimensionless period sub-interval 2 - 4.17. These results highlight specific dimensionless period band in which incident wave most amplifies. Amplification ratio values gradually mitigate for the dimensionless periods less than 2 and for those of more than 4. In addition, this agreement reveals the fact that potential amplification ratio value approximated in time-domain analyses is congruous with that calculated in spectral-domain. This conclusion paves the way to estimate the highest amount of amplification ratio in time-domain using the spectral-based results of previous studies conducted by other researchers.

There are a number of blanked areas in Tables (3) and (4). That is due to the two main reasons stated herein. First, in order to satisfy Kuhlemeyer and Lysmer element size qualifications [43], the frequency band more than 7.6 Hz (i.e. the period band less than 0.15 second) is filtered for all records. Therefore, all response spectra represented here are reliable for the periods more than 0.15 seconds. Additionally, it is convention in engineering codes to present periods up to the period 4 seconds. With all this in hand, the amplification ratios have only calculated for accurate period band - that is - 0.15 to 4 seconds.

Equation (2) is presented according to time-domain results. However, the Equation (3) is a developed form of the Equation (2) and takes the spectral amplification ratios to account. It predicts the amplification ratio of the crest of the trapezoidal-shaped hill (e.g. points *A* and *B*) for any interested period considering the various hill widths, the shape ratios, and the averaged shear wave velocity of the media (Equation 4).

$$A_{acc}\left(2D/1D\right)= \begin{cases} 1+0.8(SR)\left(\frac{1}{2}P\right), & 0.25 \le P < 2 \\ 1+0.8(SR), & 2 \le P \le 4 \\ 1+0.8(SR)\left(2-\frac{1}{4}P\right), & 4 < P \le 8 \end{cases} \quad (3)$$

$$P = \frac{Vs \ . \ T}{B} \quad (4)$$

where *SR* is the shape ratio of the trapezoidal-shaped hill, *P* is the dimensionless period, *Vs* is the averaged shear wave velocity of the site, *B* is the width of the hill, and *T* is the period the amplification ratio of which is expected to be estimated.

4. Comparing the Results with Codes

EC 8 and AFPS 90 are among the most important codes taking the topographic effects into account in their seismic designs [39-40]. EC 8 puts an aggravation factor forward considering the whole shape of the two-dimensional hill and its average slope angle. Though, AFPS 90 defines the aggravation factor considering the angles of successive surface irregularities along the hillside. Thus, the size of the hill is not mentioned in both methods to estimate the aggravation factor.

Here, the results of the numerical method extracted from the time-domain analyses, those of EC 8 and AFPS 90, and the estimated amplification factor patterns calculated by Equation (3), called "this study", are compared for different shape ratios and hill widths at the points on the hill surface and its beside as shown in Figures (10) to (13). Using Equation (3) needs three considerations: First, since the estimation of the maximum amplification ratio is required, the dimensionless period range of $2 \le P \le 4$ is selected. Second, for the ground surface points beside the hill, the amplification ratio is overestimated to be 1. Third, for the ground surface points on the slope of the hillside, the amplification ratios linearly decline from the value calculated by Equation (3) at upper edge of the slope to the value 1 at the lower edge of the slope.

All three estimating methods try to put forward a reasonable value for any point on the hill, hillside, and beside it. Nevertheless, there are some differences that are rigorously discussed hereunder. It is crystal clear how Equation (3) can reliably estimate the amplification ratio patterns when it comes to be compared with the codes. Since it has the parameters *P* and *SR*, it takes into consideration the hill-width and the height of the hill, respectively. Subsequently, its results varies for different *SR* and *B*. As expected, it presents acceptable amplification ratio patterns for almost all conditions. Comparing the estimations of two codes shows that even EC 8 is more reliable than AFPS 90. EC 8 has good agreement in shape ratios 0.5 and 0.3; however, it is

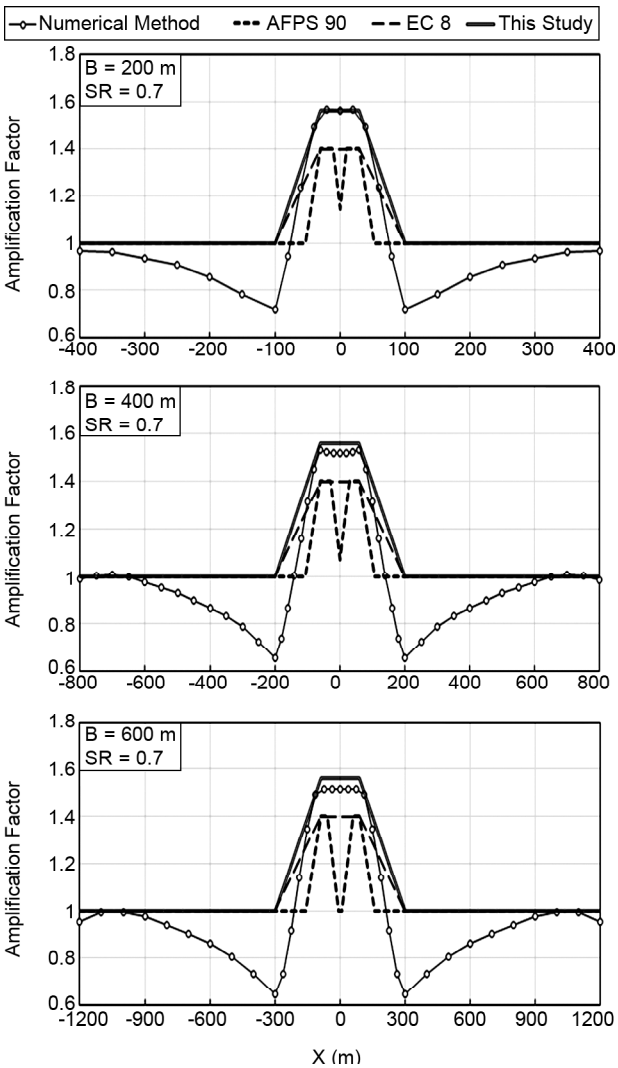

Figure 10. Comparison of the amplification ratio patterns for the trapezoidal-shaped hill with 0.7 shape ratio and various hill-widths using four methods: numerical method, AFPS 90 code, EC 8 code, and the proposed equation (this study).

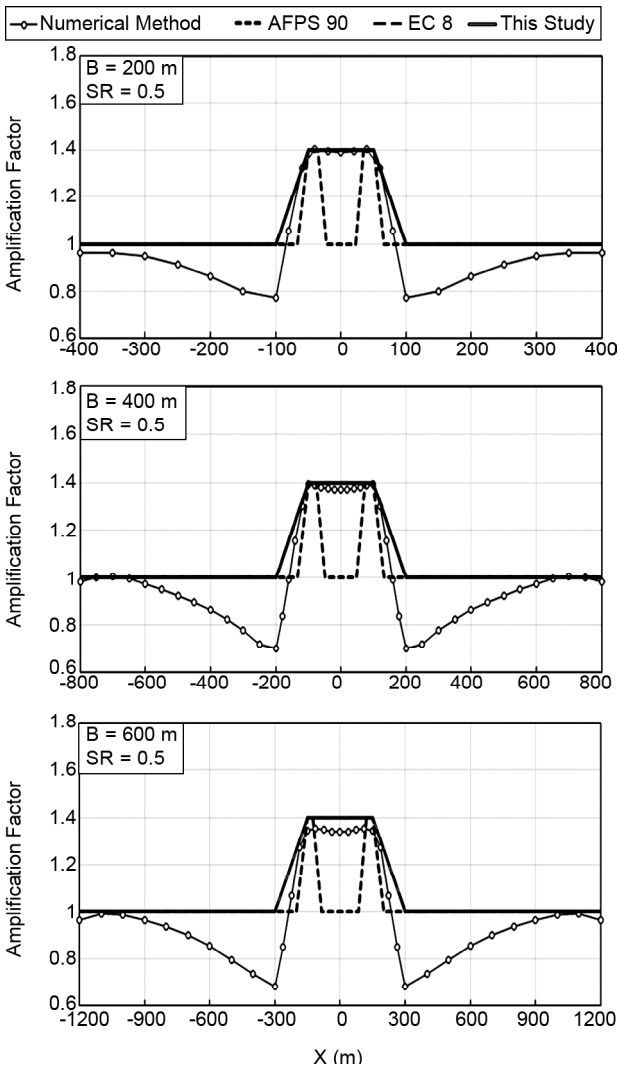

Figure 11. Comparison of the amplification ratio patterns for the trapezoidal-shaped hill with 0.5 shape ratio and various hill-widths using four methods; numerical method, AFPS 90 code, EC 8 code, and the proposed equation (this study).

not reliable for very high hills, e.g. shape ratio 0.7, and for very low hills, e.g. shape ratio 0.1. AFPS 90 only gives a decent estimation of the amplification factor for the points on the top edges of the hill. Due to the fact that its method does not involve the height of the hill, it fails to gain a reasonable agreement on the hill crest in most cases except for the shape ratio 0.5. All results of this study is limited to a specific form of surface irregularities - that is - a trapezoidal-shaped hill with a slope angle of 45 degree. In order to judge fairly among three methods to determine which one is more efficient, more studies need to be done considering different shapes of the hill, constitutive models for the media, characterizations of the media, conditions of contiguity, as it is discussed in another study [47], and so forth.

5. Conclusion

This study has conducted a seismic assessment on the trapezoidal-shaped hills with various hill-widths and shape ratios, which have been seismically analyzed under strong ground motion records. Then, their results have been discussed in terms of acceleration, velocity, and displacement, i.e. time-domain, as well as the spectral response.

Time-domain-related results have illustrated that an increase in size of the hill from 200 m to 600 m has no notable effect on the acceleration amplification ratio patterns; however, it raises the velocity and the displacement ones. When it comes to spectra-related results, this alteration becomes extensive on period intervals so that the amplification on the hill-crest as well as the de-amplification on the hill-toe have been observed over longer range of periods.

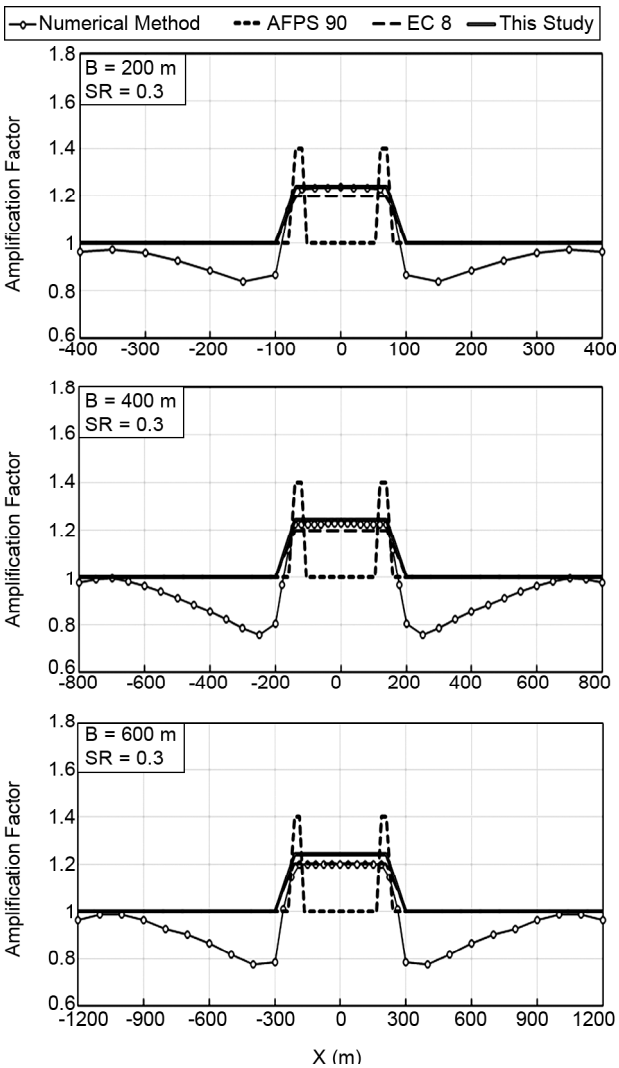

Figure 12. Comparison of the amplification ratio patterns for the trapezoidal-shaped hill with 0.3 shape ratio and various hill-widths using four methods: numerical method, AFPS 90 code, EC 8 code, and the proposed equation (this study).

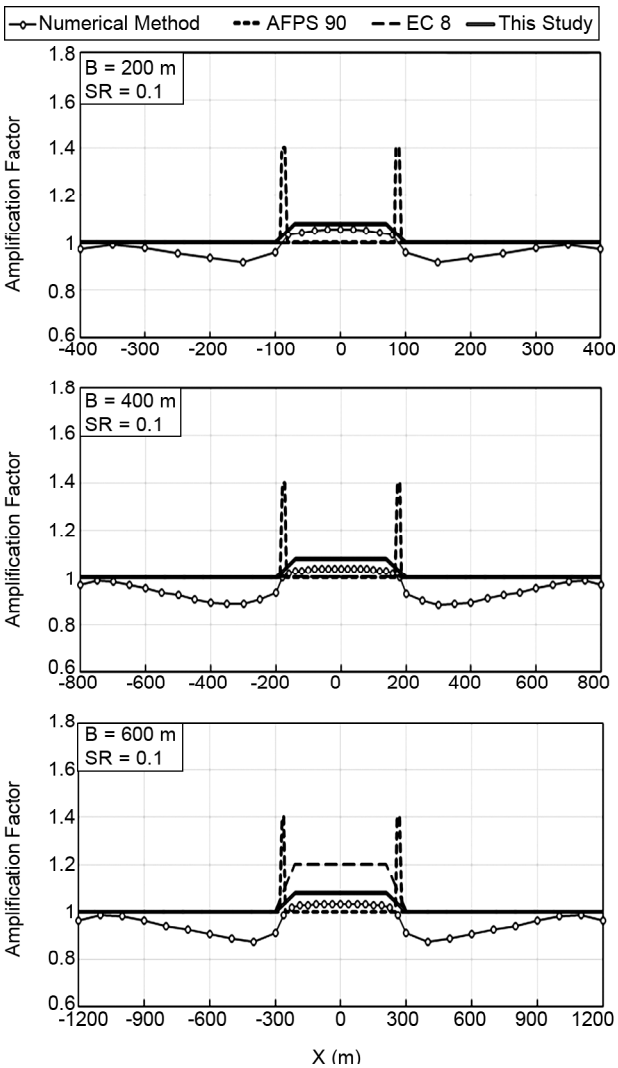

Figure 13. Comparison of the amplification ratio patterns for the trapezoidal-shaped hill with 0.1 shape ratio and various hill-widths using four methods: numerical method, AFPS 90 code, EC 8 code, and the proposed equation (this study).

Comparing the results of time-domain analyses with those of spectral ones in terms of maximum values has shown a good agreement that proves effectiveness of the previous spectral results to estimate the peak ground motion parameters; e.g. acceleration, velocity, and displacement; to be used in engineering practice. In addition, spectral analyses have revealed that topography influences the SODF oscillators with various time periods in different intensity, the most-affected of which is the time period relating to the dimensionless period interval of 2-4. Putting together the results of the numerical method extracted from the time-domain analyses, those of EC 8 and AFPS 90, and the estimated amplification factor patterns calculated by proposed equation, in this study, has proved that the suggested equation have more reliable estimation of the amplification ratio at different points on the hill, the hillside, and its beside; however, making sure of this needs more studies which consider different possibly-effective variations including the shapes of the hill, constitutive models for the media, characterizations of the media, conditions of contiguity, and so on.

References

1. Celebi, M. (1991) Topographical and geological amplification: case studies and engineering implications. *Structural Safety*, **10**(1), 199-217.

2. Celebi, M. (1987) Topographical and geological amplifications determined from strong-motion and aftershock records of the 3 March 1985 Chile earthquake. *Bulletin of the Seismological*

Society of America, **77**(4), 1147-1167.

3. Athanasopoulos, G., Pelekis, P., and Leonidou, E. (1999) Effects of surface topography on seismic ground response in the Egion (Greece) 15 June 1995 earthquake. *Soil Dynamics and Earthquake Engineering*, **18**(2), 135-149.

4. Bouckovalas, G. and Kouretzis, G. (2001) Stiff soil amplification effects in the 7 September 1999 Athens (Greece) earthquake. *Soil Dynamics and Earthquake Engineering*, **21**(8), 671-687.

5. Boore, D.M. (1973) The effect of simple topography on seismic waves: implications for the accelerations recorded at Pacoima Dam, San Fernando Valley, California. *Bulletin of the Seismological Society of America*, **63**(5), 1603-1609.

6. Trifunac, M.D. and Hudson, D.E. (1971) Analysis of the Pacoima Dam accelerogram - San Fernando, California earthquake of 1971. *Bulletin of the Seismological Society of America*, **61**(5), 1393-1411.

7. Spudich, P., Hellweg, M., and Lee, W. (1996) Directional topographic site response at Tarzana observed in aftershocks of the 1994 Northridge, California earthquake: implications for mainshock motions. *Bulletin of the Seismological Society of America*, **86**(1B), S193-S208.

8. Boore, D.M. (1972) A note on the effect of simple topography on seismic SH waves. *Bulletin of the Seismological Society of America*, **62**(1), 275-284.

9. Bouchon, M. (1973) Effect of topography on surface motion. *Bulletin of the Seismological Society of America*, **63**(2), 615-632.

10. Bard, P.Y. (1982) Diffracted waves and displacement field over two-dimensional elevated topographies. *Geophysical Journal of the Royal Astronomical Society*, **71**(3), 731-760.

11. Sanchez-Sesma, F.J. (1983) Diffraction of elastic waves by three-dimensional surface irregularities. *Bulletin of the Seismological Society of America*, **73**(6A), 1621-1636.

12. Bouchon, M. (1985) A simple, complete numerical solution to the problem of diffraction of SH waves by an irregular surface. *Journal of the Acoustical Society of America*, **77**(1), 1-5.

13. Gaffet, S. and Bouchon, M. (1989) Effects of two-dimensional topographies using the discrete wavenumber-boundary integral equation method in P-SV cases. *Journal of the Acoustical Society of America*, **85**(6), 2277-2283.

14. Sanchez-Sesma, F.J. and Campillo, M. (1991) Diffraction of P, SV, and Rayleigh waves by topographic features: a boundary integral formulation. *Bulletin of the Seismological Society of America*, **81**(6), 2234-2253.

15. Sanchez-Sesma, F.J. and Campillo, M. (1993) Topographic effects for incident P, SV and Rayleigh waves. *Tectonophysics*, **218**(1), 113-125.

16. Ashford, S.A., Sitar, N., Lysmer, J., and Deng, N. (1997) Topographic effects on the seismic response of steep slopes. *Bulletin of the Seismological Society of America*, **87**(3), 701-709.

17. Zhang, B., Papageorgiou, A.S., and Tassoulas, J.L. (1998) A hybrid numerical technique, combining the finite-element and boundary-element methods, for modeling the 3D response of 2D scatterers. *Bulletin of the Seismological Society of America*, **88**(4), 1036-1050.

18. Bouckovalas, G.D. and Papadimitriou, A.G. (2005) Numerical evaluation of slope topography effects on seismic ground motion. *Soil Dynamics and Earthquake Engineering*, **25**(7), 547-558.

19. Kamalian, M., Gatmiri, B., and Sohrabi-Bidar, A. (2003) On time-domain two-dimensional site response analysis of topographic structures by BEM. *Journal of Seismology and Earthquake Engineering*, **5**(2), 35-45.

20. Kamalian, M., Jafari, M.K., Sohrabi-Bidar, A., Razmkhah, A., and Gatmiri, B. (2006) Time-domain two-dimensional site response analysis of non-homogeneous topographic structures by a hybrid BE/FE method. *Soil Dynamics and*

Earthquake Engineering, **26**(8), 753-765.

21. Kamalian, M., Sohrabi-Bidar, A., Razmkhah, A., Taghavi, A., and Rahmani, I. (2008) Considerations on seismic microzonation in areas with two-dimensional hills. *Journal of Earth System Science*, **117**(2), 783-796.

22. Sohrabi-Bidar, A. (2008) *Seismic Behavior Assessment of Surface Topographies Using Time-Domain 3D Boundary Elements Method*. Ph.D. Thesis, International Institute of Earthquake Engineering and Seismology, Tehran, Iran.

23. Sohrabi-Bidar, A., Kamalian, M., and Jafari, M.K. (2009) Seismic waves scattering in three-dimensional homogeneous media using time-domain boundary element method., *Earth Space Phys.*, **38**(1), 23-40.

24. Sohrabi-Bidar, A., Kamalian, M., and Jafari, M.K. (2009) Time-domain BEM for three-dimensional site response analysis of topographic structures. *International Journal for Numerical Methods in Engineering*, **79**(12), 1467-1492.

25. Sohrabi-Bidar, A., Kamalian, M., and Jafari, M.K. (2010) Seismic response of 3-D Gaussian-shaped valleys to vertically propagating incident waves. *Geophysical Journal International*, **183**(3), 1429-1442.

26. Sohrabi-Bidar, A. and Kamalian, M. (2013) Effects of three-dimensionality on seismic response of Gaussian-shaped hills for simple incident pulses. *Soil Dynamics and Earthquake Engineering*, **52**, 1-12.

27. Housner, G.W. (1941) *An Investigation of the Effects of Earthquakes on Buildings*. Ph.D. Thesis, California Institute of Technology.

28. Biot, M.A. (1943) Analytical and experimental methods in engineering seismology. *Transactions of the American Society of Civil Engineers*, **108**(1), 365-385.

29. Housner, G.W. (1959) Behavior of structures during earthquakes. *Journal of Engineering Mechanics Division*, ASCE, 109-129.

30. Hayashi, S., Tsuchida, H., and Kurata, E. (1972) *Average Response Spectra for Various Subsoil Condition*. McGraw Hill Book Inc., 14.

31. Mohraz, B., Hall, W., and Newmark, N.A. (1972) *Study of Vertical and Horizontal Earthquake Spectra*. AEC Report WASH-1255, NM Newmark Consulting Engineering Services, Urbana, Illinois, USA.

32. Blume, J.A., Sharpe, R.L., and Dalal, J.S. (1973) *Recommendations for Shape of Earthquake Response Spectra*. John A. Blume and Associates.

33. Newmark, N.M., Blume, J.A., and Kapur, K.K. (1973) Design response spectra for nuclear power plants. *ASCE Structural Engineering Meeting, San Francisco*.

34. Seed, H.B., Ugas, C., and Lysmer, J. (1976) Site-dependent spectra for earthquake-resistant design. *Bulletin of the Seismological Society of America*, **66**(1), 221-243.

35. Borcherdt, R. (1991) Methodology for predictive GIS mapping of special study zones for strong ground shaking in the San Francisco Bay region, CA. *Proceedings Fourth Int. Conf. Seismic Zonation*, **3**, 545-552.

36. Borcherdt, R. (1994) Estimates of site-dependent response spectra for design (methodology and justification). *Earthquake Spectra*, **10**(4), 617-653.

37. Assimaki, D., Kausel, E., and Gazetas, G. (2005) Soil-dependent topographic effects: A case study from the 1999 Athens earthquake. *Earthquake Spectra*, **21**(4), 929-966.

38. Kamalian, M., Jafari, M.K., Sohrabi-Bidar, A., and Razmkhah, A. (2008) Seismic response of 2-D semi-sine shaped hills to vertically propagating incident waves: amplification patterns and engineering applications. *Earthquake Spectra*, **24**(2), 405-430.

39. AFPS (1990) Recommendations, Association Française du Génie Parasismique, Saint-Rémy-lès-Chevreuse France.

40. Eurocode, E.C.8 (1998) *Design Provisions for Earthquake Resistance of Structure*.

41. Wong, H. (1982) Effect of surface topography

on the diffraction of P, SV, and Rayleigh waves. *Bulletin of the Seismological Society of America*, **72**(4), 1167-1183.

42. IBC, I. (2006) *International Building Code*. International Code Council, Inc. (formerly BOCA, ICBO and SBCCI), 4051, 60478-5795.

43. Kuhlemeyer, R.L. and Lysmer, J. (1973) Finite element method accuracy for wave propagation problems. *Journal of Soil Mechanics and Foundations Division*, **99** (Tech. Rpt).

44. PEER (2000) *Strong Motion Database. Regents of the University of California*.

45. Shareghi, A., Amelsakhi, M., and Sohrabi Bidar, A. (2015) Evaluation of earthquake waves amplification due to trapezoidal hill by 1D and 2D time domain analysis. *Journal of Engineering Geology*, **8**(4), 2389-2412.

46. Amelsakhi, M., Sohrabi-Bidar, A., and Shareghi, A. (2014) Spectral assessing of topographic effects on seismic behavior of trapezoidal hill. *International Journal of Environmental, Chemical, Ecological, Geological and Geophysical Engineering, World Academy of Science, Engineering and Technology*, **8**(4), 245-252.

47. Nazari, A., Baziar, M.H., and Shahnazari, H. (2010) Seismic effects of two-dimensional semi-sine shaped hills on ground motion response. *Electronic Journal of Geotechnical Engineering*, **5**, 1159-1170.